Research in Astronomy and Astrophysics, 24:085017 (16pp), 2024 August https://doi.org/10.1088/1674-4527/ad634e

Photometric Studies of EV Cnc and AH Cnc in the Open Cluster M67

Mamatha Rani G., K. Sriram, Deblina Lahiri, and Vijaya, A.
Department of Astronomy, Osmania University, Hyderabad 500007, India; mamatharamgopal@gmail.com
Received 2024 January 25; revised 2024 April 11; accepted 2024 April 29; published 2024 August 12

Abstract

Contact binaries at various stages of evolution unveil various operating mechanisms that drive them. We report the photometric and period variation analysis of two contact binaries EV Cnc and AH Cnc in open cluster M67. We observed the cluster from the JCBT 1.3 m telescope and utilized TESS and Kepler observations. The photometric solutions of EV Cnc and AH Cnc revealed a mass ratio of $q \sim 0.41$ and $\sim$0.15 with an inclination of $i = 42°$ and 87° respectively. These solutions suggest that EV Cnc is probably a semi-detached and AH Cnc is a deep low-mass ratio contact binary. The study of $O - C$ variation analysis indicates that for both systems, the period is increasing which suggests the mass transfer is occurring from secondary to primary. In the case of AH Cnc and based on simulations by randomly varying the time of minima to fit the LITE solution, we noted the third body orbital period to be around $P_3 = 26.82 \pm 2.54$ yr, which is different from earlier reported values and conclude that future observations are required to confirm this scenario. We compare these two systems with other similar contact binaries to get an estimate of the final configuration of the respective systems.

Key words: (stars:) binaries (including multiple): close – (stars:) binaries: eclipsing – stars: activity

1. Introduction

Contact binaries are a special class of binaries where one or both of the stellar component, with F, G, and K spectral type stars, fill their Roche lobe and have dissimilar or similar surface temperatures. Massive contact binaries are also being observed with A and B spectral type stars (Li et al. 2023) and some are also seen with M spectral type (Qian et al. 2015a). The primary reason for thermal or non-thermal equilibrium among the components is due to the presence of a shared convective common envelope (CCE) located across the inner and outer equipotential surfaces (Lucy 1968). Through this envelope, both mass and energy exchange takes place driving the binary to overcontact to the marginal or semi-detached phase of the binary. The contact binaries are classified into two broad classes i.e., W and A-type (Binnendijk 1970). The evolution of these sub-types is not understood and theory predicts that they formed via angular momentum loss (AML) and are driven by quasi-magnetic activity (vant Veer 1979; Qian et al. 2017, 2018) and finally merge to form a rapidly rotating star.

It was predicted that these systems undergo a thermal relaxation oscillation (TRO, Lucy 1976; Lucy & Wilson 1979) which explains the exclusive state of marginal contact binaries or semi-detached binaries. As the contact binary evolves toward this state, the stellar components have high-temperature differences reflected as unequal minima in the light curves and are observed to be associated with a shallow CCE. Moreover, a secular mass transfer from the secondary to the primary component drives the binary to a marginal contact state. It was predicted that this oscillation has a thermal timescale of $\sim 10^7$ yr due to non-thermal equilibrium.

The AML driven by magnetic activity plays a key role in the evolution of contact binaries (vant Veer 1979; Rahunen 1981; Vilhu 1982; Guinan & Bradstreet 1988; van't Veer & Maceroni 1989). When the system is in a contact stage the magnetic activity induces a torque that drives the binary to form a low-mass ratio system with hotter components, further decreasing the efficiency. The efficiency decreases since as the system evolves toward a shorter orbital period, the magnetic activity lowers and hence the AML mechanism slowly ceases due to magnetic braking (Qian 2001). On the other hand, the secular mass transfer from the secondary to the primary would increase the orbital period further decreasing the density of the CCE. Moreover, the primary component will become massive, further shallowing the CCE and magnetic activity restarts (Maceroni & van't Veer 1996). This mechanism will make the system evolve toward a marginal contact binary and drive toward a semi-detached configuration. It is clear that the conservation of angular momentum (AM) is not a physically feasible scenario and hence Rahunen (1981) reported a hypothetical critical AML rate of about $2 \times 10^{-9}\,\mathrm{yr}^{-1}$. If the observed AML is more than the critical AML, the system will coalesce to form a single star, and if it is less then the system will oscillate back to a marginal contact state.

Since these systems oscillate, a critical mass ratio must exist where the secular mass transfer changes from primary to secondary and vice-versa. Qian (2001) showed that such a mass ratio is observed based on a study of contact binaries and found

q to be around $q = 0.4$. The $q < 0.4$ systems tend to display a period decrease in the $O - C$ diagram whereas the orbital period was found to increase in high mass ratio systems viz. $q > 0.4$. Based on a catalog of Kepler eclipsing binary systems, Kouzuma (2018) reported that a process of mass transfer from primary (massive) to secondary becomes rapid while it slows when the mass transfer occurs from secondary to primary when both AML and mass loss mechanisms were considered. Kouzuma (2018) also noted a critical mass ratio $q = 0.5$ where the mass transfer and loss trend display opposite behavior.

Ev Cnc is a short period semi-detached binary system with an orbital period of $P = 0.44124$ day (Gilliland 1991). It is a partially eclipsing binary system and exhibits an ellipsoidal variation in the light curve possibly due to the mutual tidal effects and this system emits X-ray probably from the magnetically active component via the stellar coronae (van den Berg et al. 2002). The earlier light curve displays asymmetry at the maxima probably caused by the hot spot activity (Yakut et al. 2009). $O - C$ studies show that the orbital period was found to be increasing in EV Cnc with a rate of $dp/dt = 2.4 \times 10^{-6}$ days yr^{-1}, which is relatively high and further observations are needed to confirm it. We studied this system for a few basic reasons viz. (1) EV Cnc mass ratio was estimated to be $q = 0.4$–0.5 with sparse data and we would like to confirm the result (Yakut et al. 2009); (2) To determine more robustly the rate of change of period, i.e., dp/dt and constrain the mass transfer and mass loss rates. On the other hand, AH Cnc is a well studied contact binary system with a low mass ratio configuration (Qian et al. 2006; Yakut et al. 2009). The $O - C$ variation exhibits the presence of a third body along with a period increasing trend. In the present work, a detailed analysis of photometric solutions and an $O - C$ diagram analysis are performed for both EV Cnc and AH Cnc, and their probable final binary configurations are discussed.

2. Data Reduction and Analysis

The sources EV Cnc and AH Cnc were observed from the JCBT 1.3 m telescope at Vainu Bappu Observatory (VBO), IIA, equipped with a 2k × 2k CCD during 2018 March 8th, 2019 February 2 and 3, 2022 March 31 and 2022 April 24 and 2023 February 9 with an exposure time of 300 s in the V band. It should be noted that we used 2019 year data for photometric solutions as in other nights, but we did not obtain complete phase light curves, however, we obtained the times of minima from other night data. We used the *apphot* IRAF package to perform differential photometry (e.g., Sriram et al. 2016). We also used Kepler K2 (EPIC 211412192) and Transiting Exoplanet Survey Satellite (TESS) (TIC 437039183) data to model the light curves and estimate the photometric solutions. Further, the data were used to obtain the times of minima to perform the study of the $O - C$ diagram.

3. Photometric Solutions of EV Cnc

EV Cnc is an interesting source as its location is close to the turn-off point of the cluster (Yakut et al. 2009). The light curve exhibits a difference between the primary and secondary minima closely resembling a semi-detached or a marginal contact binary system. Generally, these systems have a high-temperature difference (e.g., Qian et al. 2020). We noted that the Kepler light curve displays an asymmetry in the maxima at phases 0.25 and 0.75, which is also observed in the JCBT light curve. Since the source has not been explored in terms of a photometric solution except by Yakut et al. (2009), we again determine the various photometric solutions using JCBT, Kepler, and TESS light curves. The Phoebe software (Prsa & Zwitter 2005) was invoked to perform the photometric analysis which uses primarily the Wilson–Devinney (WD) methodology (Wilson & Devinney 1971; Wilson 1979, 1990). We adopted the following procedure to get the best solution for the light curves (for more details see Sriram et al. 2016, 2017, 2018). The gravity darkening coefficient $g_1 = g_2 = 0.32$ was fixed (Lucy 1967) along with the adopted albedos $A_1 = A_2 = 0.5$ for both components (Ruciński 1969). We fixed the primary temperature $T_1 = 6900$ K (Yakut et al. 2009). Bandpass and bolometric limb darkening coefficients (square root) were adopted from the table determined by van Hamme (1993). A circular and synchronous ($F = 1$) orbit was assumed. Four parameters were adjusted initially, i.e., temperature of the secondary component (T_2), orbital inclination (i), the dimensionless potentials of the primary and secondary components (Ω_1, Ω_2) (depending on the configuration), and the respective bandpass luminosity of the primary star (L_1). We attempted non-thermal contact, semi-detached primary (SD1) and secondary (SD2) filled Roche lobe configurations to obtain the solutions. Since there is no spectroscopic mass ratio available for this source, we adopted a grid search method to constrain it. The grid search was performed in the range of $0.04 < q < 5$ by varying the adjustable parameters (Figure 1, top panel). Later the mass ratio parameter was also freed to get the best fit (Figure 1, bottom panel). It is clear that the SD2 configuration resulted in the lowest residual among the three trial solutions. The best-fit solution resulted in a mass ratio of $q = 0.410 \pm 0.007$. Table 1 displays solutions for thermally decoupled contact and SD2 (for comparison) best-fits for the observed light curves for JCBT, Kepler, and TESS data. Figure 2 displays the best fit for JCBT (top), Kepler (middle), and TESS (bottom) light curves. It can be vividly seen that all light curves display asymmetry and we fitted a hot and a cool spot over the cooler component which decreased the residuals (Figure 2, Table 1). Such a hot spot region was also observed by Yakut et al. (2009). The size of the hot spot ($25° \pm 4°$) is noted to be larger than that of the cool spot ($18° \pm 2°$). The hot spot could be due to the impact of the material over the stellar surface causing the increase in the temperature of that region.

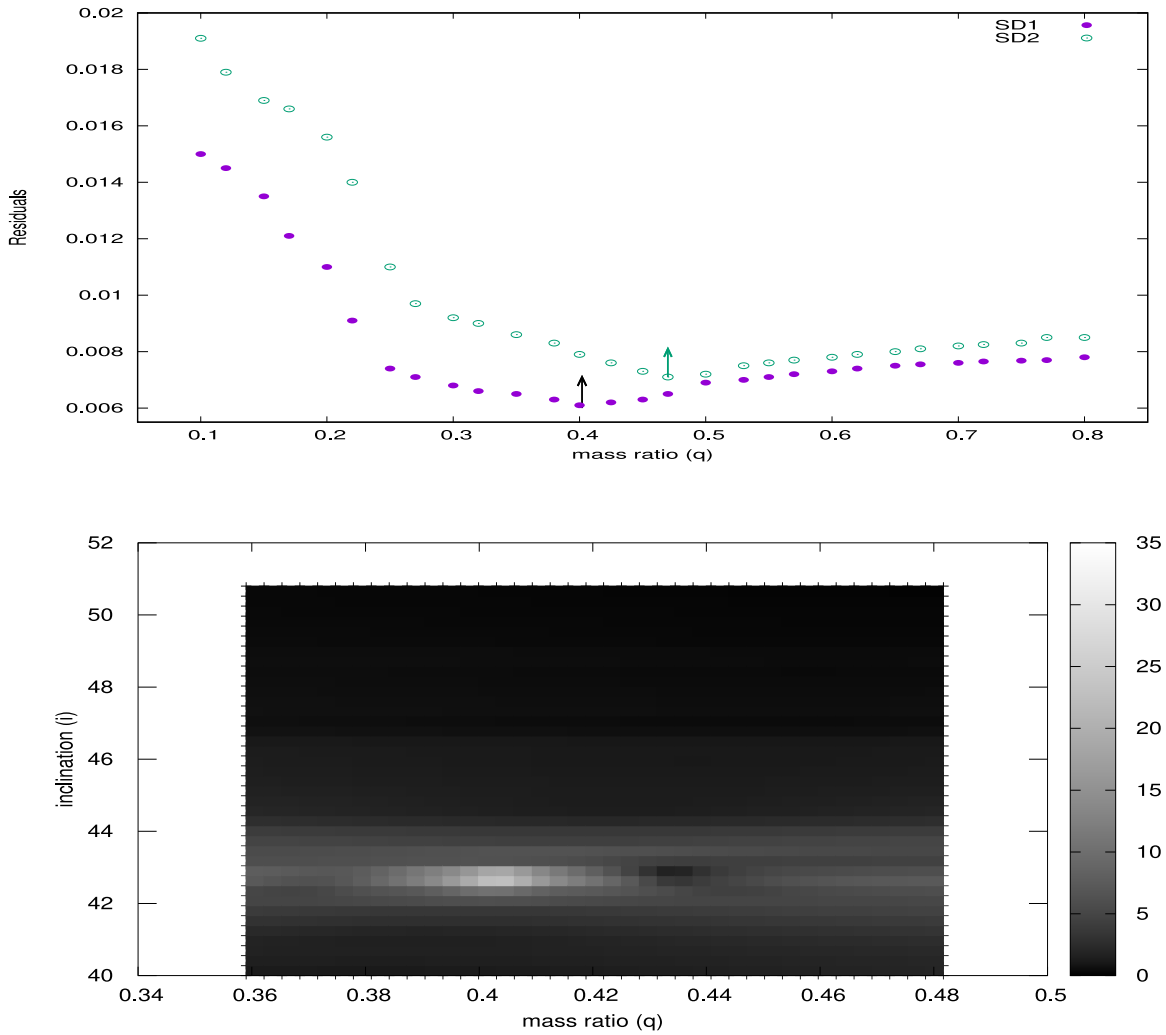

Figure 1. Top panel displays the residual variation as per the grid search method for the semi-detached (SD, mode 4) configuration. The arrow marks show the residuals for SD1 (Primary Roche lobe fill) and SD2 (Secondary Roche lobe fill). Bottom panel: density plot for mass ratio vs. inclination after running the Pheobe program in the selected grid.

4. Period Variation

The $O-C$ diagram of EV Cnc displays period variation and earlier studies found that the period is increasing with a rate of dp/dt==2.4×10^{-6} days yr^{-1}. With new times of minima, we studied the period variation of EV Cnc. Table 2 displays the log of all times of minima and Figure 3 displays the $O-C$ diagram using JCBT times of minima and the period of the binary is found to be consistently increasing. A parabolic equation was fitted which resulted in the following equation using a least-squares solution for JCBT times of minima.

$$\begin{aligned}\mathrm{Min}.I = {} & 0.0022(0.0001) + 2.40(0.01) \times 10^{-7} \\ & \times E + 1.44(0.01) \times 10^{-10} \times E^2(\mathrm{JCBT}). \end{aligned} \quad (1)$$

The secular increase in the period (using JCBT Min. I) with a rate of $dp/dt = 2.28 \times 10^{-7}$ days yr^{-1} was observed. The increase in the period suggests that mass transfer is taking place from the secondary to the primary component and is determined from the following Equation (2)

$$\frac{\dot{P}}{P} = 3\dot{M}_1\left[\frac{1}{M_1} - \frac{1}{M_2}\right]. \quad (2)$$

The mass of the primary component was found to be 1.31 $M_\odot$ and is derived from Equation (3) (Kılıcoglu 2021)

$$\bar{M} = a\bar{T} + b10^{c\bar{T}} + d\bar{g}10^{e\bar{g}}, \quad (3)$$

where:

$\bar{M} = \log(M/M_\odot)$v,
$\bar{T} = \log T_{\mathrm{eff}}$–4,
$\bar{g} = \log g$–4.

Table 1
Best-fit Photometric Solutions Obtained for EV Cnc

Parameters	JCBT C	JCBT SD2	KEPLER K2 C	KEPLER K2 SD2	TESS C	TESS SD2
$A_1 = A_2$	0.5	0.5	0.5	0.5	0.5	0.5
$g_1 = g_2$	0.32	0.32	0.32	0.32	0.32	0.32
T_1(K)	6900	6900	6900	6900	6900	6900
T_2(K)	5630 ± 18	5200 ± 15	5630 ± 18	5200 ± 15	5630 ± 18	5200 ± 15
q (m_2/m_1)	0.693 ± 0.003	0.410 ± 0.002	0.692 ± 0.003	0.418 ± 0.002	0.693 ± 0.003	0.423 ± 0.002
i^o	45.33 ± 0.12	42.95 ± 0.13	46.7 ± 0.12	42.91 ± 0.12	46.71 ± 0.12	42.08 ± 0.03
$\Omega_1 = \Omega_2$(C), Ω_1(SD2)	3.3100 ± 0.0055	2.7012 ± 0.0087	3.3308 ± 0.0087	2.7108 ± 0.0055	3.3018 ± 0.0087	2.6914 ± 0.0055
r_1 (pole)	0.4301	0.4389	0.3725	0.4325	0.3773	0.4398
r_1 (point)	…	0.5121	…	0.5025	…	0.5134
r_1 (side)	0.4585	0.4717	0.3907	0.4622	0.3966	0.4716
r_1 (back)	0.4852	0.5081	0.4146	0.4920	0.4224	0.5034
r_2 (pole)	0.2860	0.3086	0.2890	0.3098	0.2886	0.3028
r_2 (point)	…	0.3711	…	0.3789	…	0.3751
r_2 (side)	0.2984	0.3241	0.2880	0.3298	0.2887	0.3286
r_2 (back)	0.3322	0.3666	0.3381	0.3611	0.3287	0.3686
$L_1/(L_1 + L_2)$	0.85	0.41	0.86	0.40	0.86	0.41
Spot Parameters Two spots on secondary						
colatitude (θ°)	86 ± 5, 52 ± 3	86 ± 5, 52 ± 3	87 ± 6, 55 ± 4	87 ± 5, 55 ± 3	86 ± 5, 55 ± 3	86 ± 5, 55 ± 4
longitude (ζ°)	12 ± 3, 193 ± 11	12 ± 3, 193 ± 12	11 ± 2, 190 ± 11	11 ± 2, 190 ± 10	11 ± 2, 193 ± 11	11 ± 2, 193 ± 11
Radius (°)	14 ± 2, 24 ± 3	18 ± 2, 25 ± 4	12 ± 2, 22 ± 4	12 ± 2, 22 ± 4	12 ± 2, 25 ± 4	12 ± 2, 25 ± 4
Temp. ratio	1.12 ± 0.08	1.12 ± 0.08	1.22 ± 0.18	1.22 ± 0.19	1.20 ± 0.16	1.20 ± 0.16
	0.78 ± 0.05	0.78 ± 0.06	0.81 ± 0.07	0.81 ± 0.07	0.80 ± 0.07	0.80 ± 0.07
$\Sigma w(o-c)^2$	0.0087	0.0062	0.0069	0.0059	0.0070	0.0060

Note. Model C is for non-thermal contact and model SD2 for semi-detached, in which the secondary star fills its Roche lobe.

The coefficients are given as:

$a = +0.769687,$
$b = +0.409173,$
$c = +0.611016,$
$d = -0.204335,$
$e = -0.175664.$

The mass transfer rate was found to be $1.54 \times 10^{-8}\, M_\odot\, \mathrm{yr}^{-1}$. Moreover, it is possible that mass loss can occur from either of the companions which further increases the period of the system. The mass loss can be estimated from the following Equation (3) (Tout & Hall 1991; Kouzuma 2018)

$$\dot{M}_1 = -\frac{M_1 + M_2}{2}\frac{\dot{P}}{P}. \quad (4)$$

The mass loss rate $\dot{M}_1$ was found to be $4.47 \times 10^{-7}\, M_\odot\, \mathrm{yr}^{-1}$. The distance to the source is found to be 2793 ly or 856 pc based on Gaia parallax measurement which is close to the distance of the M67 cluster and it indicates that EV Cnc is a member of the cluster.

5. Photometric Solution of AH Cnc

We obtained the data in the V band as discussed above for the overcontact binary system AH Cnc. One can see a total eclipse which helps us to constrain the mass ratio more accurately than other partially eclipsing binaries. We use Phoebe software for the analysis of the light curve of the system which uses the WD code in Mode 3 (Wilson & Devinney 1971; Wilson 1990). Based on the color index B–V, the adopted value for the primary star was $T_1 = 6300$ K, gravity darkening coefficients were taken as $g_1 = g_2 = 0.32$ (Lucy 1967), and adopted values for albedos were $A_1 = A_2 = 0.5$ (Ruciński 1969). The logarithmic limb-darkening coefficients (x_1, x_2) were obtained from van Hamme (1993). The following parameters were made to vary during the fitting procedure, q (mass ratio), L_1, (V band luminosity), the surface potential of the primary component Ω, T_2 and inclination i°. After many iterations, we finally achieved the best fit for the observed light curve (see Figure 4 and Table 3). We noted a filling factor of $f = \Omega_{\mathrm{in}} - \Omega/\Omega_{\mathrm{in}} - \Omega_{\mathrm{out}}$ to be 0.55, i.e., 55% of the Roche lobe is filled and AH Cnc has a high degree of contact which is essential for the criteria of the merger scenario.

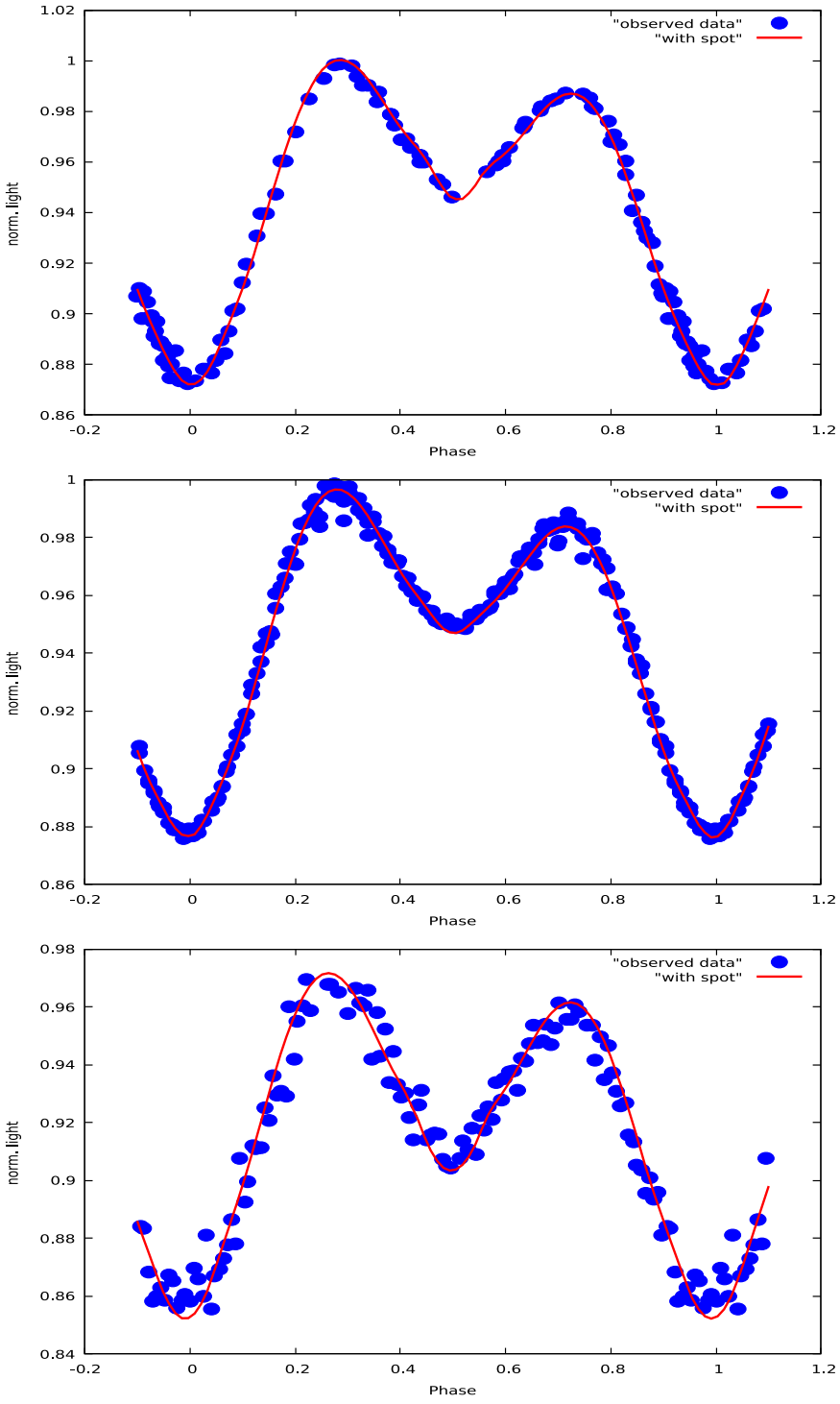

Figure 2. Best fit solutions for semi-detached mode for JCBT (top), Kepler (middle), and TESS (bottom) light curves.

Previous studies revealed that the light curve solution sometimes needs a spot over the primary, however, we did not see such type of solution in our light curves in the present study.

6. Results and Discussion

The EV Cnc light curve displays a temperature difference of $\sim$1700 K and the photometric mass ratio is noted to be $q = 0.41$.

Table 2
Log of Times of Minima for the Source Ev Cnc

HJD(2400000+)	Epoch	$O-C$	Reference
51229.7723	−16511	0.003433	(1)
51231.7441	−16506.5	0.019655	(1)
51250.7368	−16463.5	0.030439	(1)
51603.2028	−15665	0.006679	(2)
51604.0883	−15663	0.009299	(2)
52244.6052	−14212	−0.003095	(3)
52246.6091	−14207.5	0.0143251	(8)
53108.2776	−12255.5	−0.007859	(4)
53109.1864	−12253.5	0.018060	(8)
53425.4532	−11537	−0.006827	(5)
53426.3392	−11535	−0.003707	(5)
53443.345	−11496.5	0.006656	(6)
53682.6029	−10954.5	0.004130	(5)
54144.128	−9909	0.003815	(7)
54147.2024	−9902	−0.011864	(7)
54147.6584	−9901	0.002695	(7)
54150.3054	−9895	0.001056	(7)
54151.6301	−9892	0.001436	(7)
54152.0721	−9891	0.001996	(7)
54152.5075	−9890	−0.004043	(7)
54513.395	−9072.5	0.006338	(8)
55235.802	−7436	−0.003057	(8)
55621.3991	−6562.5	−0.003710	(8)
55621.409	−6562.5	0.006189	(8)
55621.4146	−6562.5	0.011789	(8)
56015.38	−5670	−0.007921	(8)
57142.5989	−3116.5	−0.005795	(9)
57144.8092	−3111.5	−0.002675	(9)
57145.2496	−3110.5	−0.003715	(9)
57145.692	−3109.5	−0.002814	(9)
57147.0159	−3106.5	−0.003174	(9)
57148.3392	−3103.5	−0.004274	(9)
57150.1058	−3099.5	−0.003363	(9)
57152.3151	−3094.5	−0.0013334	(9)
57156.7259	−3084.5	−0.004852	(9)
58186.3872	−752	−0.0021492	(10)
58517.247	−2.5	−0.001597	(10)
58518.3502	0	−0.002	(10)
59552.6453	2343	−0.000525	(11)
59554.8538	2348	0.000803	(11)
59573.1747	2389.5	0.001858	(11)
59578.2513	2401	0.001979	(11)
59670.291	2609.5	0.001376	(12)
59694.3495	2664	0.001483	(12)
59985.2588	3323	0.001808	(12)
59985.4804	3323	0.002778	(12)

References. (1) Blake (2002); (2) Csizmadia et al. (2002); (3) Csizmadia et al. (2006); (4) Krajci (2005); (5) Yakut et al. (2009); (6) Hübscher et al. (2005); (7) Pribulla et al. (2008); (8) Bob Nelson's Database; (9) Kepler K2 Data; (10) Tess Data; (11) JCBT; (12) TESS.

We attempted various solutions and noted that the best-fit solution suggests that the secondary component filled its Roche lobe. Recently Xiong et al. (2024) studied TESS sectors 1–26 and found 77 semi-detached binaries with an orbital period ranging from 18.75 to 0.37 days and there were only 10–11 SD systems whose periods are lying in the range of 0.4–0.5 day. It clearly suggests that such low AM, i.e., tight SD, systems are rare among binaries. The orbital period for EV Cnc is still far away from the lower limit $P_{\rm min} = 0.248$ days for SDs for A-F stars (Zhai et al. 1989), which is further validated by Xiong et al. (2024). This kind of system can be considered as a prototype which connects the classical Algol and Contact binaries. EV Cnc $O-C$ variation strongly indicates an increasing trend in the orbital period with $dp/dt = 2.28 \times 10^{-7}$ days yr^{-1} which is almost ten times lower than the previously reported rate of period change (Yakut et al. 2009) but still, the observed period change is similar to that generally seen in these types of systems. In general, SD2 type systems have a lower degree of variation in the period when compared to the classical Algol (Wang et al. 2022). In the case of EV Cnc, as the secondary Roche lobe is filled, the material will transfer to the primary's surface, further increasing the orbital period and decreasing the mass ratio. This phenomenon shall drive the system toward the classical Algol configuration. Qian et al. (2018) studied the distribution of thousands of Algol/SD2 type binaries and found a peak around ∼0.7 day, below which the number of such systems drastically decreases. It is also possible that the mass of the secondary component would decrease which is due to the mass loss phenomenon. It is quite possible that as the convective layer depth decreases the magnetic winds would enable the secondary mass to escape via the winds and hence the mass ratio may further lower.

Since both conservative mass transfer and AML are important driving mechanisms occurring in these systems, it can be concluded that TRO is ongoing. Generally, this oscillation occurs over a duration of a few million years (Qian 2001). As the geometric contact lowers, the CCE depth decreases. As the CCE slides off, the respective stellar activity will increase its strength and cause the material to go off from the stellar surface. Later the AML increases, which decreases the orbital period and the mass transfer would take place from primary to secondary. This will lead the binary to evolve toward contact configuration via the marginal contact binary phase. Overall the mutual inter-dependent mechanisms of mass transfer and AML control the evolution of these systems. Assuming that this period variation is due to conservative mass transfer from the secondary to the primary component, then the mass transfer rate is found to be around $\dot{M} = 2.28 \times 10^{-8}\, M_{\odot}\, {\rm yr}^{-1}$. We used Gazea's three-dimensional relation (Gazeas et al. 2009) to calculate the mass and radius. One can estimate the mass transfer timescale or oscillation timescale which is of the order of $M_2/\dot{M} = 23.2$ Myr and the corresponding period increase timescale is $P/\dot{P} = 1.93$ Myr.

The asymmetry in the light curve indicates the presence of spots over the secondary based on our solutions. Previous studies by Yakut et al. (2009) also reported the presence of

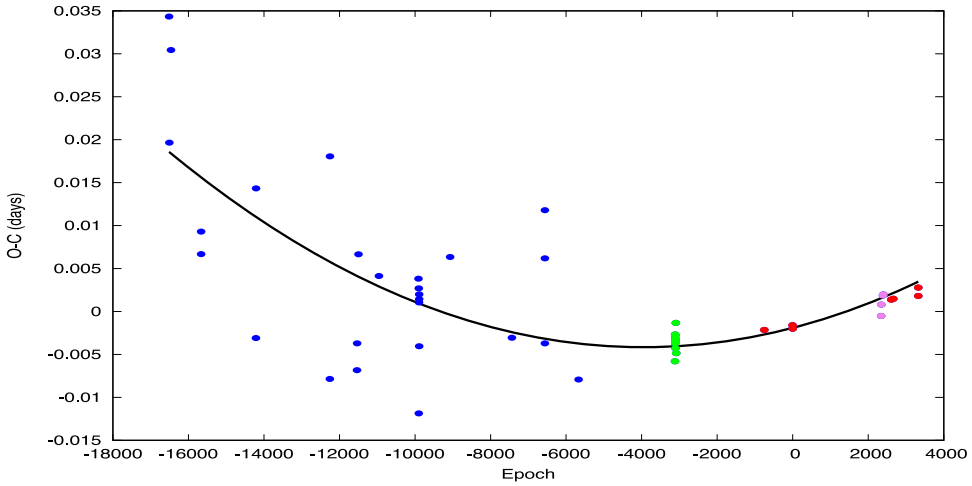

Figure 3. The $O-C$ variation using the JCBT (red) times of minima. Green and purple points display the Kepler K2 and TESS data respectively.

spots over the cool star. This suggests that stellar activity is also triggering the AML from the system. This would tend to drive the system toward the contact configuration rather than the semi-detached phase. The AML via the magnetic winds can be calculated using the following equation (Bradstreet & Guinan 1994)

$$\dot{P}_{\rm AML} \approx -1.1 \times 10^{-8} q^{-1}(1+q)^2(M_1+M_2)^{-5/3}k^2 \times (M_1R_1^4 + M_2R_2^4)P^{-7/3}, \quad (5)$$

where the gyration constant is $k^2 \sim 0.07$ to 0.20 for solar-type stars. By adopting a value of $k^2 = 0.1$ (Bradstreet & Guinan 1994) and assuming $M_1 = 1.31\,M_\odot$, $M_2 = 0.53_\odot$, $R_1 = 1.43_\odot$, $R_2 = 1.17_\odot$ and $q = 0.41$, the rate of orbital period decrease due to AML can be computed as $\dot{P}_{\rm AML} = -1.76 \times 10^{-9}$ days yr^{-1}. This results in a period variation timescale of $P_{\rm orb}/\dot{P}_{\rm AML} = 0.025 \times 10^9$ yr ~ 25 Myr. This timescale is much longer than the timescale deduced assuming conservative mass transfer which was 1.93 Myr. Hence we conclude that the EV Cnc is driven by the process of mass transfer from secondary to primary component though it has magnetic activity. Although the stellar winds might be present, the magnitude is not enough to drive the system to the contact phase. Cohen et al. (2009) showed in their simulations that the spot location on the stellar component can control the AML. Our photometric solution suggests that spots were located close to the equator. As per their simulations if the spots are lying close to the poles, then it would trigger a relatively higher AML than if the spots would have been located at the equator. It has also been found that the AML somehow controls the stellar dynamo and hence the magnetic field structure over the stellar surface. Kouzuma (2019) studied a small sample of semi-detached binary systems and noted that the size of the hot spot increases with decreasing mass ratio in the range of $0.2 \leqslant q \leqslant 0.6$ and is often seen in the star whose temperature is greater than 6000 K. It was concluded that the mass transfer should occur primarily from their spots. Further studies on the spot location and its variation and their movement require more precise photometric observations.

In this study, we obtained times of minima for AH Cnc using JCBT, Kepler, and TESS data, and others were collected from the literature (Table 4). This is to date the largest times of minima collected for this source. Using JCBT times of minima, the best-fit updated quadratic solution is found to be

$$\text{Min.I} = 0.341(0.005) + 2.28(0.06) \times 10^{-6} \times E + 2.42(0.01) \times 10^{-10} \times E^2. \quad (6)$$

The $O-C$ variation is plotted versus Epoch (Figure 5 top panel). The variations suggest that the period is increasing and follows a parabolic variation. The increase in the period indicates the mass transfer in this system. The period is increasing at a rate of $\dot{P} = 4.1 \times 10^{-7}$ days yr^{-1} in AH Cnc which is higher than that reported by Yakut & Ibanoglu (2000) ($\dot{P}_{\rm Yakut} = 2.4 \times 10^{-6}$ days yr^{-1}), whereas Qian et al. (2006) reported a $\dot{P} = 4.00 \times 10^{-7}$ days yr^{-1}. On the other hand, Peng et al. (2016) reported a $\dot{P} = 4.29 \times 10^{-10}$ days yr^{-1}. Mass is being transferred from a low mass component to a more massive component. Earlier studies strongly indicate that AH Cnc has a possible presence of a third body (Qian et al. 2006; Pribulla & Rucinski 2006; Yakut et al. 2009).

To fully determine the different parameters of the third body assuming the cyclic variation is caused due to a third body (i.e., LITE, see Equation (6)), we used Zasche's code (Zasche et al. 2009) which implements the Simplex method to find best-fit solutions. A blue line is used to show the period-increasing quadratic term only, and a red line displays the following equation applied in the overall $O-C$ diagram in Figure 5 top

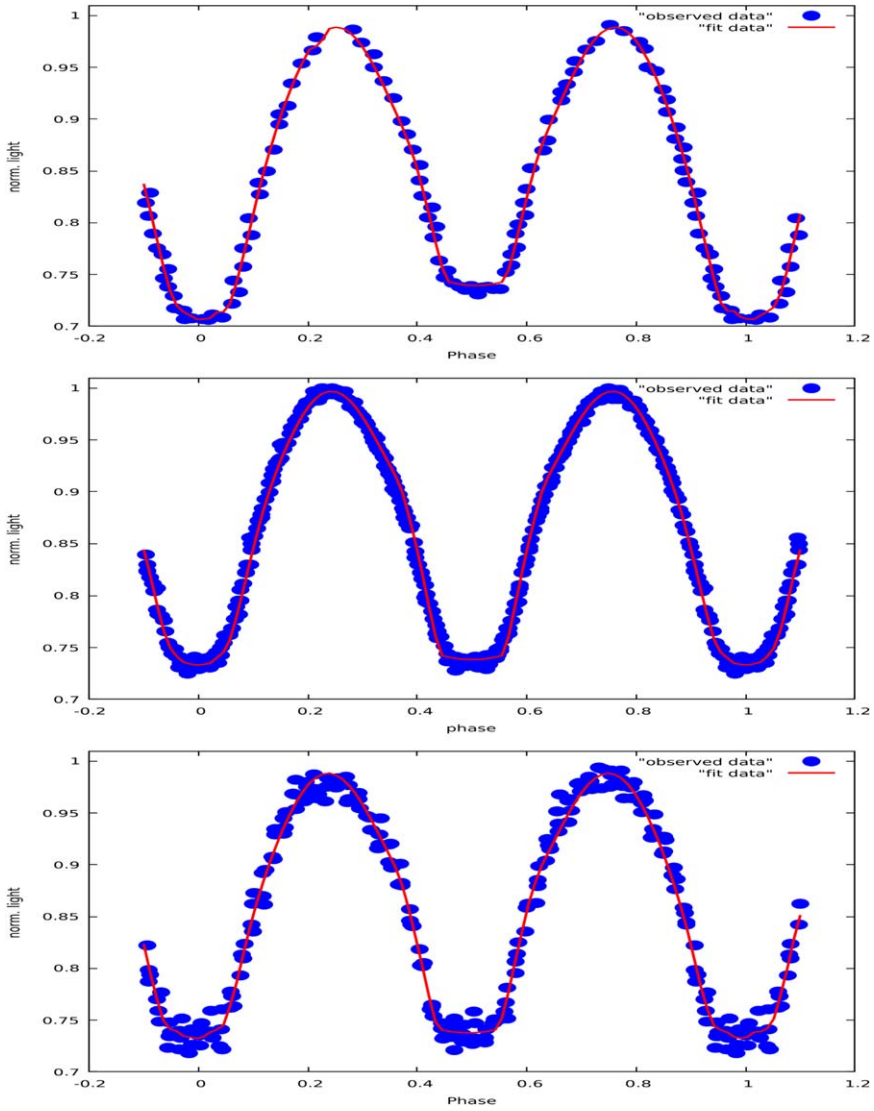

Figure 4. The best fit of JCBT phased light curve (top panel), Kepler (middle panel), and TESS (bottom panel) for AH Cnc. The circles represent the data and the thick line displays the fits.

panel.

$$\text{Min.I} = JD_o + P.E + Q.E^2 + \frac{a_{12}\sin i}{c} \times \left[\frac{1-{e_3}^2}{1+e_3\cos\nu}\sin(\nu+\omega_3) + e_3\sin(\omega_3)\right], \quad (7)$$

where the projected semimajor axis, speed of light, eccentricity, the true anomaly of the binary orbit around the triple system's center of mass, and the longitude of the periastron are, respectively, represented by a_{12} sin$i$, c, e_3, ν, and ω_3. JD_o is the starting epoch for the primary minimum, E is the integer eclipse cycle number, P is the orbital period of the binary, $Q = 1/2 \times (dP/dt)$, which is a measure of the rate of change of the period. During the fitting procedure, different parameters were left free and allowed the program to get the lowest residual. Initially, we constrained the eccentricity to be fixed at $e_3 = 0.68$ (Yakut et al. 2009) but later kept it free to obtain the uncertainty. The mass transfer in the Zasche code was obtained from the parabolic curve as discussed above (Figure 5 top panel). The best-fit estimated parameters along with error bars are shown in Table 5. The third body period was found to be $P_3 = 24.58 \pm 1.22$ yr along with an eccentricity $e_3 = 0.33 \pm 0.12$. It can be noticed that the previously reported third body period is different than that estimated in the present study. Yakut et al. (2009) reported a period of ∼34 yr whereas Qian et al. (2006) estimated it to be 36.5 yr along with another companion with a period of 7.75 yr. With more times of minima, Peng et al. (2016) reported a value of 35.26 yr assuming a circular orbit of the third body. To robustly calculate the orbital

Table 3
Best-fit Photometric Solutions Obtained for AH Cnc

Parameters	JCBT	Kepler K2	TESS
Albedo, $A_1 = A_2$	0.5	0.5	0.5
Gravity brightening, $g_1 = g_2$	0.32	0.32	0.32
T_1(K)	6300	6300	6300
T_2(K)	6212 ± 18	6234 ± 12	6201 ± 15
q (m_2/m_1)	0.157 ± 0.003	0.137 ± 0.002	0.147 ± 0.002
fill-out factor, f (%)	60	55	53
i^o	87.25 ± 0.12	87.29 ± 0.11	88.40 ± 0.027
$\Omega_1 = \Omega_2$	2.03036 ± 0.0087	2.03036 ± 0.00094	2.0307 ± 0.0055
r_1 (pole)	0.5287	0.5238	0.5261
r_1 (side)	0.5905	0.5815	0.5858
r_1 (back)	0.6195	0.6044	0.6116
r_2 (pole)	0.2612	0.2518	0.2601
r_2 (side)	0.2654	0.2587	0.2510
r_2 (back)	0.2545	0.2512	0.2489
$L_1/(L_1 + L_2)$	0.81	0.80	0.80
$\Sigma w(o - c)^2$	0.0012	0.0011	0.0010

period, we ran the computation by considering all the times of minima and estimated the best solutions for the third body orbital period and eccentricity (For more details, see Sriram & Mamatha Rani 2023). Histograms were obtained and each of them was fitted with a Gaussian function. Figure 6 top panel displays the histogram for the orbital period (P_3) along with the best fit Gaussian line shown with a thick line and the lower panel shows the same for eccentricity (e_3). The best fit resulted in a third body period of $P_3 = 26.82 \pm 2.54$ yr. Similarly, the eccentricity was found to be $e_3 = 0.69 \pm 0.07$. The uncertainties are at the 90% confidence level ($\chi^2 = 2.71$).

AH Cnc is an important source due to its low mass ratio. These types of systems are predicted to merge due to instability. The coalescence into a single star from a binary system is theoretically well explored but lacks observational evidence. The low mass ratio eclipsing binary systems of EW light-curve type (EWs) provide laboratories to study and understand the merger scenario and challenge the current models (Eggleton 2010, and references therein). There is hardly any binary source that merged and was observed. In at least one case, V1309 Sco, such a merger event has been directly observed (Nakano et al. 2008). This defined a distinct new class of luminous red novae that was later attributed, upon analysis of archival photometric data from the Optical Gravitational Lensing Experiment (OGLE; Udalski 2003), to the merging components of a cool overcontact eclipsing binary system with a decreasing orbital period (Tylenda et al. 2011). What triggers the binary to merge is still controversial. The widely accepted scenario is Darwin's instability model (Darwin 1879). When the binary is in contact configuration, the binary will merge and form a single star if the spin AM of stellar components is more than one-third of the orbital AM, i.e., $J_{\rm spin} \geqslant 1/3\ J_{\rm spin}$ (Hut 1980; Rasio 1995).

Generally, this scenario is possible if the mass ratio of the binary system is low ($q \leqslant 0.2$) and the secondary component is small and less massive. In these circumstances, the secondary star synchronicity with the primary breaks down due to the tidal interaction. Due to this phenomenon, with higher spin velocity, the respective AM is transferred to the surface of the primary and eventually spins up the primary component. This causes the orbit of the binary to shrink and the period starts to decrease, eventually leading to the merger. So the question arises, if the merger is not seen as observational, then is there any indirect evidence for such a mechanism to be proved? It is believed that FK Com and blue straggler-type stars could be the result of this coalescence process due to their high spin and a special location in the Hertzsprung-Russell (HR) diagram (Rasio 1995; Stepien 2006; Stepien & Kiraga 2015). Other possible physical processes may trigger the merger. Both AM and mass loss from the binary due to the stellar winds and the presence of a third body companion/companions help in tightening the binary, slowly evolving the binary toward coalescence (Stepien & Gazeas 2012). Actually, the frequency of the contact binary is often seen to be high and most of them host a third body, clearly indicating that such tight binaries with low AM are possible (Rucinski et al. 2007; Raghavan et al. 2010; Rappaport et al. 2013). There is another source, KIC 9832227 (Molnar et al. 2017), which shows a large period change of the order of $\sim 10^{-6}$ days yr^{-1} which is 10–100 times faster when compared with normal period change often seen in contact binaries.

In addition, both the loss of mass and AM through magnetic winds (Stepien 2006; Stepien & Gazeas 2012) and the presence of other companion(s) plays a crucial role in the merging

Table 4
Available Times of Minima for AH Cnc Along with Other Parameters

Sr. No.	HJD(2400000+)	Epoch	$O-C$	$(O-C)_{\rm residual}$	Sr. No.	Minima	Epoch	$O-C$	$(O-C)_{\rm residual}$
1	33626.364	−72252.5	2.422509	0.97	41	51939.1468	−21448	0.169602	0.022636
2	34421.307	−70047	2.388553	0.933722	42	51940.2221	−21445	0.18638	0.016565
3	35219.318	−67833	2.347511	0.892924	43	51940.2277	−21445	0.170844	0.022165
4	36656.352	−63846.5	1.882059	0.784865	44	51940.2278	−21445	0.170567	0.022265
5	37378.322	−61843.5	1.825251	0.759494	45	51956.9876	−21398.5	0.173584	0.020815
6	37699.3	−60953	1.761565	0.762535	46	51957.1642	−21398	0.18364	0.017186
7	38820.785	−57841.5	1.821615	0.67358	47	51958.0662	−21395.5	0.181207	0.018044
8	39964.3	−54669	1.737915	0.458518	48	51958.2465	−21395	0.180998	0.018115
9	40329.398	−53656.5	1.307159	0.593806	49	51959.1478	−21392.5	0.180507	0.018272
10	40570.94	−52986.5	1.253831	0.600016	50	52314.1944	−20407.5	0.169541	0.014727
11	40678.323	−52688.5	1.247869	0.416201	51	52314.2001	−20407.5	0.153727	0.020428
12	41396.332	−50696.5	1.203038	0.394857	52	52314.2001	−20407.5	0.153727	0.020428
13	41740.7166	−49741	1.243509	0.362794	53	52315.0943	−20405	0.172937	0.013485
14	41740.908	−49740.5	1.212489	0.373965	54	52315.1	−20405	0.157123	0.019185
15	41742.89	−49735	1.213637	0.373452	55	52315.2771	−20404.5	0.165792	0.016057
16	41752.804	−49707.5	1.208282	0.374885	56	52315.2771	−20404.5	0.165792	0.016057
17	41797.675	−49583	1.218395	0.368988	57	52995.2842	−18518	0.114909	0.021026
18	41815.698	−49533	1.215475	0.369138	58	52996.364	−18515	0.119212	0.019455
19	42537.3	−47531	1.208614	0.336224	59	52997.2642	−18512.5	0.12178	0.018513
20	43163.554	−45793.5	1.23777	0.296187	60	53001.229	−18501.5	0.122204	0.018285
21	43192.214	−45714	1.223917	0.299855	61	53004.1135	−18493.5	0.119713	0.01913
22	43256.371	−45536	1.227768	0.295509	62	53004.2951	−18493	0.115898	0.020501
23	43931.492	−43663	1.184867	0.280548	63	53005.1948	−18490.5	0.119854	0.019059
24	44015.288	−43431	0.703081	0.270296	64	53005.3747	−18490	0.120756	0.01873
25	47200.699	−34593.5	0.709101	0.142558	65	53006.2758	−18487.5	0.120827	0.018688
26	47200.879	−34593	0.709717	0.14233	66	53007.1818	−18485	0.107304	0.023545
27	47203.762	−34585	0.711258	0.141674	67	53008.2609	−18482	0.113548	0.021274
28	47203.944	−34584.5	0.706325	0.143445	68	53009.3435	−18479	0.110083	0.022503
29	50904.288	−24319	0.199234	0.035883	69	53047.3702	−18373.5	0.112317	0.020989
30	51159.3059	−23611.5	0.197159	0.030456	70	53083.054	−18274.5	0.114488	0.019547
31	51177.1469	−23562	0.200478	0.028834	71	53083.054	−18274.5	0.114488	0.019547
32	51177.3275	−23561.5	0.199436	0.029206	72	53084.1348	−18271.5	0.116016	0.018976
33	51179.33	−23556	0.19851	0.029492	73	53084.1348	−18271.5	0.116016	0.018976
34	51229.7727	−23416	0.199571	0.027912	74	53380.2541	−17450	0.090442	0.02285
35	51231.749	−23410.5	0.216679	0.021698	75	53426.3926	−17322	0.088182	0.022854
36	51245.8122	−23371.5	0.20084	0.027076	76	53426.3931	−17322	0.086795	0.023354
37	51250.6798	−23358	0.196553	0.028506	77	53437.7466	−17290.5	0.088729	0.022459
38	51273.0268	−23296	0.198792	0.027172	78	53439.1867	−17286.5	0.093453	0.020731
39	51585.1847	−22430	0.172855	0.02931	79	53439.1874	−17286.5	0.091511	0.021431
40	51939.1411	−21448	0.185416	0.016936	80	53439.1876	−17286.5	0.090956	0.02163

Sr. No.	Minima	Epoch	$O-C$	$(O-C)_{\rm residual}$	Sr. No.	Minima	Epoch	$O-C$	$(O-C)_{\rm residual}$
81	53439.1886	−17286.5	0.088182	0.022631	116	57155.9219091	−6975.5	0.207912	0.083804
82	53442.7929	−17276.5	0.088756	0.02236	117	57156.6457537	−6973.5	0.215933	0.08669
83	53471.0831	−17198	0.103132	0.016686	117	57156.6457537	−6973.5	0.215933	0.08669
84	53471.0879	−17198	0.089815	0.021486	118	57160.64926	−6962.5	0.215103	0.086363
85	53471.0896	−17198	0.085099	0.023186	119	57162.77198	−6956.5	0.2117	0.085121
86	53489.2928	−17147.5	0.083886	0.023307	120	57164.575158	−6951.5	0.214273	0.086036
87	53683.5814	−16608.5	0.068377	0.025585	121	57165.4758343	−6949	0.213063	0.085593
88	53750.6235	−16422.5	0.073324	0.022683	122	57166.378524	−6946.5	0.217402	0.087151
89	53765.3982	−16381.5	0.083844	0.018646	123	57179.716948	−6909.5	0.221797	0.088641
90	54060.9837	−15561.5	0.04076	0.029406	124	57180.4416	−6907	0.26935	0.091828
91	54173.4445	−15249.5	0.040853	0.027622	125	57182.2425657	−6902	0.271493	0.091043
92	54513.3642	−14306.5	0.0025	0.036371	126	57184.94424	−6895	0.223767	0.089315
93	54831.836	−13423	0.032184	0.044411	127	57185.84708	−6892	0.271617	0.090973
94	54883.7412	−13279	0.03244	0.043803	128	57186.56658	−6890.5	0.224474	0.089559
95	54946.6421	−13104.5	0.037966	0.044956	129	57192.33516	−6874	0.271842	0.090846
96	55567.0004	−11383.5	0.092002	0.056759	130	57195.399512	−6865.5	0.270353	0.091362

Table 4
(Continued)

Sr. No.	HJD(2400000+)	Epoch	$O-C$	$(O-C)_{\rm residual}$	Sr. No.	Minima	Epoch	$O-C$	$(O-C)_{\rm residual}$
97	55621.42772	−11232.5	0.088991	0.055052	131	57197.2020533	−6860.5	0.269721	0.091577
98	55621.42812	−11232.5	0.090101	0.055453	132	57200.0863016	−6852.5	0.267879	0.092221
99	55621.42922	−11232.5	0.093153	0.056553	133	57212.165305	−6819	0.25741	0.095912
100	55621.4321	−11232.5	0.101198	0.059452	134	58186.3872	−4116.5	0.001513	0.00254
101	55621.4323	−11232.5	0.101753	0.059653	135	58517.5418932	−3198	0.209523	0.077386
102	55621.4325	−11232.5	0.102308	0.059853	136	58518.6259711	−3195	0.217103	0.080115
103	55621.433	−11232.5	0.103695	0.060353	137	59500.4180890918	−471	0.035215	−0.01265
104	55621.4331	−11232.5	0.103972	0.060453	138	59501.1403793171	−469	0.031369	−0.01126
105	55625.4152	−11221.5	0.151462	0.077526	139	59503.3072537738	−463	0.01983	−0.0071
106	55649.3804	−11155	0.137814	0.072335	140	59506.1894761608	−455	0.023866	−0.00856
107	55660.7209	−11123.5	0.099619	0.05844	141	59509.071697325	−447	0.027902	−0.01002
108	56001.7214	−10177.5	0.132487	0.066618	142	59513.3984907609	−435	0.024246	−0.0087
109	56736.344	−8139.5	0.182512	0.077852	143	59516.2807265059	−427	0.028004	−0.01006
110	57140.60142	−7018	0.204623	0.082726	144	59518.8087596241	−420	0.014682	−0.00526
111	57142.9437278	−7011.5	0.202809	0.082056	145	59521.6909914999	−412	0.018718	−0.00671
112	57150.333911	−6991	0.20526	0.082887	146	59670.20595	0	0.02122	0
113	57151.0547356	−6989	0.204958	0.082773	147	59694.00531	66	0.025626	0.009238
114	57154.120536	−6980.5	0.210332	0.084689	148	59985.25875	874	0.036739	0.013382
115	57154.48013	−6979.5	0.207962	0.083831	149	59985.48044	874.5	0.151791	0.054853

process. Since most stars are in binaries, and a significant fraction are in triples or higher order systems (Rucinski et al. 2007; Raghavan et al. 2010; Rappaport et al. 2013), potential stellar mergers may serve as keys to the binary fate. On the other hand, as orbital variations are common in contact binaries, the orbital period decay at a high rate induced by a third star proved to be crucial in the case of the recently claimed red nova precursor KIC 9832227 (Molnar et al. 2017) after the revision of its period variations (Socia et al. 2018; Kovacs et al. 2019). This system is a contact binary with an orbital period $P = 0.4579$ day, considered to be a red nova precursor. It harbors a distant low-mass companion with an orbital period of 13.5 yr. Other binary systems display large period changes. A steep period decrease of $dp/dt = -3.4 \times 10^{-6}$ days yr^{-1} over 11 yr was seen in ASAS J102556+2049.3 (Kjurkchieva et al. 2019). V1222 Tau has one of the largest period variations of $dp/dt = -8.9 \times 10^{-6}$ days yr^{-1} and an extreme O'Connell effect. Like in many low-mass ratio (LMR) systems, the long-term period variations are associated with the presence of an additional component (Pribulla & Rucinski 2006) that plays a particular role in AM evolution.

The low-mass ratio systems with high fill-out factors are known as deep low-mass ratio (DLMR; Yang & Qian 2015) systems and are potential sources of mergers. Based on the $O-C$ variation, 35 such binaries have been identified as low-mass ratio systems (Pietrukowicz et al. 2017). A bigger sample was surveyed by Hajdu et al. (2019) using the OGLE IV archive and ∼1000 systems were noted out of 80,000 with cyclic observations. Christopoulou et al. (2022) increased the sample size of LMR systems based on the Catalina Sky Survey data. Among 30 systems, 12 were found to be associated with high fill-out factors with mass ratio $q \leqslant 0.25$, and out of them, eight have very low mass ratio $q \leqslant 0.1$. For the sample, the mean primary and secondary masses were found to be $\sim 1.42\,M_{\odot}$ and $\sim 0.77\,M_{\odot}$ along with a temperature range of 5000–6500 K. It was concluded that there is no bias toward A or W sub-types of W UMa systems. We have listed the LMR systems in the period range of ∼0.30–0.40 day (Table 6). In Table 6, the columns are organized as follows: Period (in days); mass ratio ($q = M_2/M_1$); mass ratio determination method photometric with total eclipses (T) or spectroscopic (SP); primary mass (M_1); primary radius (R_1); secondary radius R_2; fill-out factor (f); the derived ratio of total spin angular to orbital momentum for gyration radii $k = 0.06$; and the derived ratio of total spin angular to orbital momentum for different values of the massive component and for the less massive component (this work). It is noticed that one system closely resembles the AH Cnc physical configuration i.e., CSS J155637.0+060949 (Christopoulou et al. 2022). This source has a similar period of $P = 0.36052$ day and displays a large period change of the order $dp/dt \sim 10^{-6}$ days yr^{-1} in nine years of CSS data. Now an interesting question arises if this system has a similar physical and radiative configuration (i.e., similar orbital period, mass ratio, primary and secondary component temperature) to that of AH Cnc, then what causes the large period change? It could be possible that there is some other mechanism that is triggering the binary to spiral down. Maybe a larger magnetic activity, causing huge stellar winds viz. a thousand times stronger winds often seen in these types of

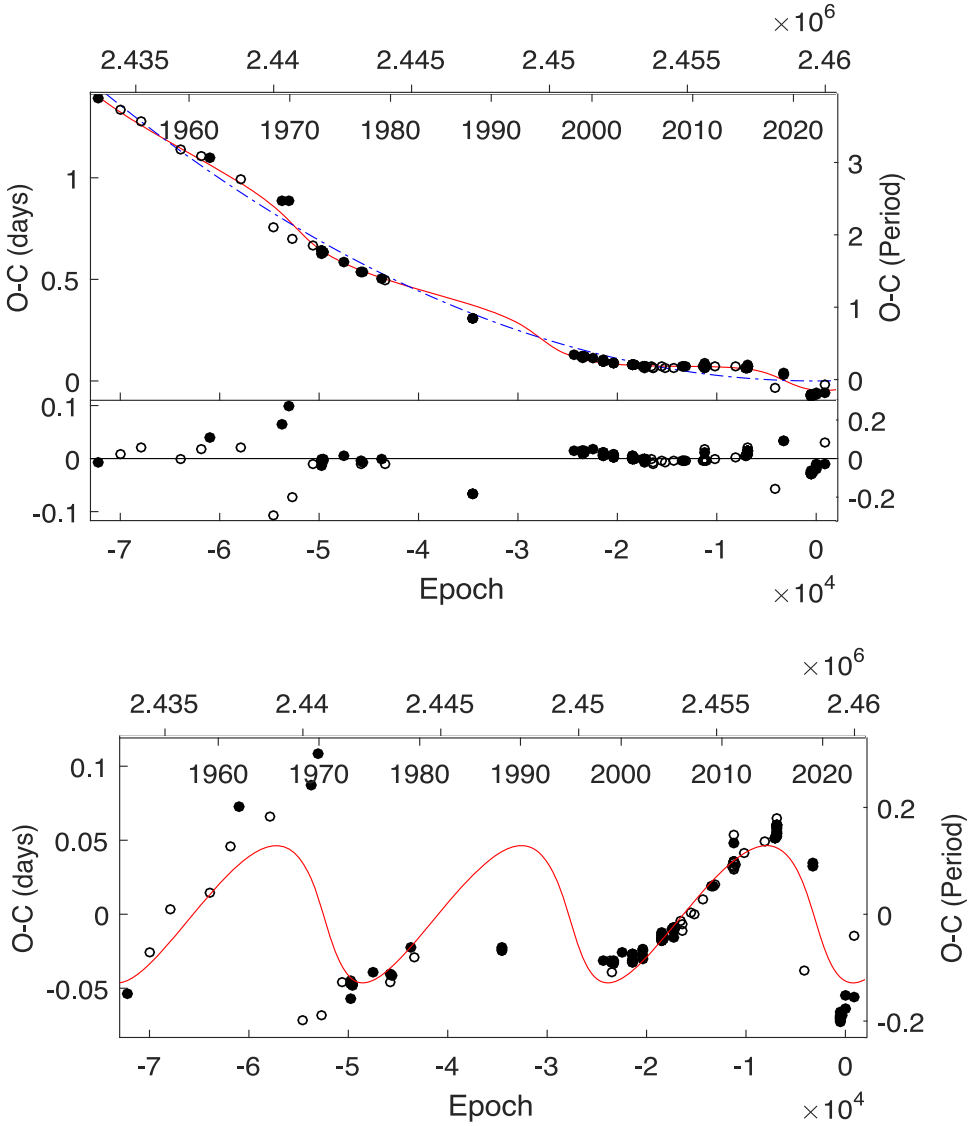

Figure 5. Third-body solution based on $O-C$ diagram using an epoch (TESS). The top panel displays the $O-C$ (circles) along with the best fit corresponding to the LITE solution (red line) and the blue line shows the parabolic fit. The lower subpanel depicts the residuals after the best fit. The bottom panel shows a zoomed view of the best fit of the third body obtained after the parabolic fit to the $O-C$.

systems $\sim 10^{-6}$–$10^{-7}\,M_{\odot}\,\mathrm{yr}^{-1}$, is removing the total AM driving the systems toward merger. Future studies are required to focus on such DLMR systems to explore the underlying mechanism observationally and theoretically.

We calculated the ratio of spin AM to orbital AM using the equation shown below

$$\frac{J_s}{J_o} = \left(\frac{1+q}{q}\right)(k_1 r_1)^2 \left(1 + q\left[\frac{k_2}{k_1}\right]^2 \left[\frac{r_2}{r_1}\right]^2\right), \tag{8}$$

where $k1$ and $k2$ are the dimensionless gyration radii of both components, and q is the mass ratio. The exact values of $k1$ and $k2$ are difficult to calculate as they depend on the structure of each stellar component, but the main sequence star has a value of 0.075 for full radiative configuration and 0.205 for fully convective configuration. For Sun-like systems ${k_1}^2 = {k_2}^2 = k^2 = 0.06$. For $k = 0.06$, the ratio for ${k_1}^2 = 0.06$ was estimated to be $(J_s/J_o) = 0.134$ and $(J_s/J_o) = 0.141$ for ${k_1}^2$ for the massive component, i.e., 0.705 and ${k_2}^2 = 0.205$. These ratios are still slightly far away from Darwin's instability criterion of $J_s/J_o = 0.33$ but secular period decrease and occasional mass loss from the systems would trigger AH Cnc to merge, forming a rapidly rotating star. It should be noted that AH Cnc shows a period-increasing trend and may eventually tend to evolve toward

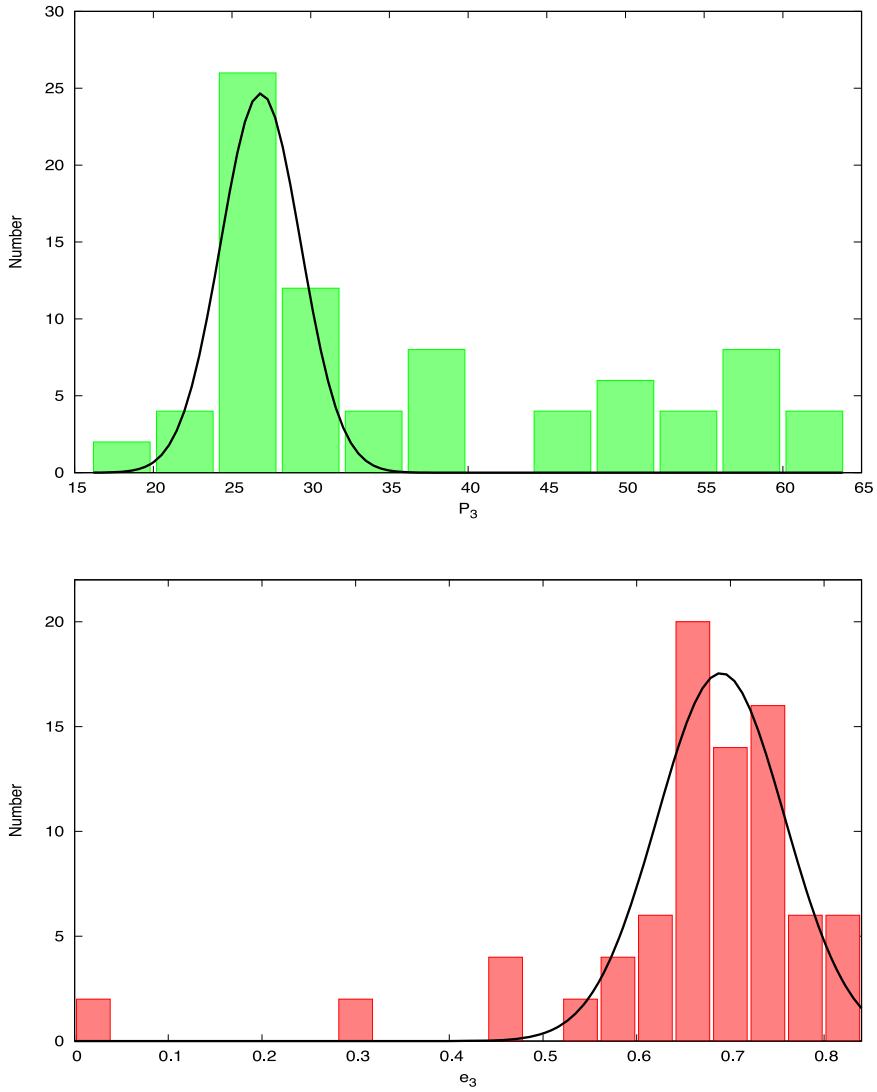

Figure 6. Top panel shows the histogram for the third body orbital period obtained by randomly varying epochs along with the best fit using a Gaussian function with a mean of $\mu = 26.82$ yr and $\sigma = 2.54$ yr. A similar histogram is for the eccentricity with $\mu = 0.69$ yr and $\sigma = 0.07$ yr.

Table 5
Best Fit Parameters of the Third Body Using LITE Solution for AH Cnc

Parameters	HJD = 2459670.2685
A, semi. amplitude (days)	0.045 ± 0.002
P_3, period (years)	24.52 ± 1.22
e_3 , eccentricity	0.33 ± 0.12
ω_3 , longitude of periastron passage	182.98 ± 14.11
T_o , time of periastron passage	2458506 ± 415
a_{12} sin$i$, (au)	8.53 ± 0.46
Q (10^{-10})	2.42 ± 0.01
$f(M_3)$, $(M_\odot)$	0.078 ± 0.00012
$M_3(M_\odot)_{i=90°}$	0.78 ± 0.0051
$M_3(M_\odot)_{i=60°}$	1.12 ± 0.0036
$M_3(M_\odot)_{i=30°}$	1.841 ± 0.001
Sum of squared residuals	0.0116

a period-decreasing trend. Future photometric studies are essential to study the period variation in AH Cnc.

The number of low mass ratio binary systems in clusters is small. For example, QX And is a short-period contact binary in the open cluster NGC 752 with a mass ratio $q = 0.23$ and has a cluster age of ∼2 Gyr (Qian et al. 2007), EP Cep in NGC 188 with $q = 0.18$ has an age of ∼5–6 Gyr (Chen et al. 2016), Tx Cnc in M44 with a $q = 0.45$ has an age of ∼0.3–0.5 Gyr, KIC 4937217 in NGC 6819 with $q = 0.26$ has an age of 2.2 Gyr (Li & Liu 2021), and KIC 9470175 and KIC 9532591 with $q = 0.24$ and 0.43 in NGC 6811 have an age of ∼1 Gyr (Li et al. 2020). V12 is a contact binary with mass ratio $q = 0.26$ in an open cluster NGC 7789 with an age of ∼1.6 Gyr (Qian et al. 2015b). It can be observed that low mass ratio CBs are

Table 6
LMR Sources in a Period Range of ∼0.30–0.40 day

Name	Period (days)	q	type	M_1 ($M_\odot$)	R_1 ($R_\odot$)	R_2 ($R_\odot$)	f	$\frac{J_s}{J_o}$	$\left(\frac{J_s}{J_o}\right)_k$	Reference
AH Cnc	0.36046	0.156	T	1.188	1.332	0.592	0.510	0.134	0.141	Present work
CSSJ155637.0+060949	0.36052	0.120	T	1.26	1.43	0.61	0.880	0.205	0.182	Christopoulou et al. (2022)
NSVS 1926064	0.40747	0.16	T	1.558	1.605	0.755	0.708	0.146	0.089	Kjurkchieva et al. (2020)
V902 Cep	0.32870	0.162	T	1.077	1.208	0.563	0.470	0.139	0.178	Kjurkchieva et al. (2019)
NSVS 2256852	0.34888	0.162	T	0.950	1.18	0.52	0.170	0.134	0.210	Kjurkchieva et al. (2019)
V972 Her	0.44309	0.164	SP	0.910	1.35	0.59	0.01	0.129	0.215	Selam et al. (2018)
V1115 Cas	0.32329	0.164	T	1.049	1.181	0.548	0.424	0.137	0.184	Kjurkchieva et al. (2019)
EPIC 211957146	0.35502	0.17	T	1.050	1.1	0.23	0.642	0.136	0.183	Sriram et al. (2017)
AS CrB	0.38066	0.172	T	1.250	1.4	0.67	0.592	0.133	0.126	Liu et al. (2017)
ASAS J002821-1453.3	0.40266	0.173	T	1.330	1.49	0.6	0.397	0.132	0.102	Gezer & Bozkurt (2016)
BO Ari	0.31819	0.19	SP	0.995	1.09	0.515	0.494	0.118	0.176	Gürol et al. (2015)
	0.31819	0.207	SP	1.095	1.19	0.636	0.757	0.113	0.147	Poro et al. (2021)
V619 Peg	0.38872	0.19	T	2.020	1.642	0.811	0.521	0.118	0.079	Kjurkchieva et al. (2019)
HV UMa	0.35539	0.19	SP	2.800	2.62	1.18	0.770	0.107	0.077	Csák et al. (2000)
V1853 Ori	0.38300	0.19	T	1.200	1.36	0.66	0.333	0.114	0.121	He et al. (2019)
NSVS 9045055	0.35459	0.202	T	1.990	1.51	0.751	0.302	0.108	0.073	Kjurkchieva et al. (2019)
UY UMa	0.37602	0.206	T	1.151	1.342	0.696	0.606	0.112	0.131	Kim et al. (2019)
TYC 2402-0643-1	0.39943	0.208	T	0.860	1.22	0.67	0.220	0.103	0.188	Samec et al. (2020)
NSVS 6859986	0.38357	0.208	T	1.870	1.63	0.84	0.860	0.115	0.078	Kjurkchieva et al. (2019)
GM Dra	0.33875	0.21	SP	1.213	1.252	0.606	0.230	0.105	0.110	Gazeas et al. (2005)
MM Com	0.30199	0.215	T	0.790	0.99	0.35	0.240	0.095	0.184	Kjurkchieva et al. (2019)
V816 Cep	0.31141	0.219	T	2.830	1.576	0.836	0.511	0.103	0.080	Kjurkchieva et al. (2019)
YY CrB	0.37656	0.232	SP	1.393	1.385	0.692	0.228	0.091	0.070	Gazeas et al. (2005)
YY CrB	0.37656	0.243	SP	1.430	1.43	0.81	0.634	0.104	0.098	Gazeas et al. (2005)
V789 Her	0.32004	0.236	T	1.130	1.15	0.62	0.238	0.091	0.114	Li et al. (2018)
HR Boo	0.31597	0.241	T	1.210	1.17	0.62	0.180	0.090	0.098	Kjurkchieva et al. (2019)
T-Dra0-00959	0.32933	0.245	T	0.890	1.06	0.5	0.240	0.084	0.147	Kjurkchieva et al. (2019)
KIC 4244929	0.34140	0.059	T	1.481	1.521	0.477	0.809	0.439	0.227	Senavcı et al. (2016) (Se)
KIC 9151972*	0.38680	0.059	T	1.606	1.696	0.528	0.760	0.438	0.231	Senavcı et al. (2016) (Se)
ASAS J083241+2332.4	0.31132	0.065	T	1.220	1.34	0.42	0.506	0.398	0.354	Sriram et al. (2016)
ZZ PsA	0.37388	0.078	T	1.213	1.422	0.559	0.970	0.298	0.284	Wadhwa et al. (2021b)
M4 V53	0.30845	0.078	T	1.472	1.383	0.481	0.690	0.320	0.168	Li et al. (2017)
SX Crv	0.31660	0.079	SP	1.246	1.347	0.409	0.272	0.303	0.283	Zola et al. (2004)
V870 Ara	0.39972	0.082	SP	1.503	1.61	0.61	0.984	0.310	0.166	Szalai et al. (2007)
KR Com	0.40797	0.093	SP	0.880	1.445	0.505	0.990	0.286	0.489	Gazeas et al. (2021)
UCAC4 479-113711	0.35292	0.1	T	1.400	1.47	0.58	0.893	0.204	0.119	El-Sadek et al. (2019)
ASAS J165139+2255.7	0.35321	0.103	T	1.030	1.27	0.46	0.600	0.216	0.291	Alton (2018)
FG Hya	0.32783	0.104	SP	1.445	1.438	0.515	0.698	0.244	0.134	Zola et al. (2010)
GR Vir	0.34697	0.106	SP	1.376	1.49	0.55	0.932	0.232	0.167	Gazeas et al. (2005)
V1191 Cyg	0.31339	0.107	SP	1.283	1.292	0.503	0.577	0.221	0.184	Ostadnezhad et al. (2014)
CK Boo	0.35515	0.111	SP	1.584	1.533	0.65	0.946	0.221	0.125	Deb & Singh (2011)
TYC 6995-813-1 (n)	0.38318	0.111	T	1.230	1.46	0.6	0.720	0.243	0.223	Wadhwa et al. (2021b)
NSVS 3198272	0.35228	0.115	T	1.621	1.479	0.583	0.391	0.198	0.111	Kjurkchieva et al. (2019)
KIC 6118779	0.36425	0.117	T	1.465	1.512	0.657	0.922	0.209	0.118	Senavcı et al. (2016)
KIC 10395609	0.36425	0.121	T	1.460	1.504	0.657	0.916	0.167	0.093	Senavcı et al. (2016)
ASAS J040633-4729.4	0.40637	0.136	T	1.330	1.54	0.6	0.324	0.164	0.127	Saygan (2016)
DZ Psc	0.36613	0.136	SP	1.370	1.46	0.67	0.987	0.179	0.129	Yang et al. (2013)
HV Aqr	0.37450	0.14	SP	1.240	1.456	0.601	0.740	0.175	0.163	Gazeas et al. (2021)
V710 Mon	0.40520	0.143	T	1.140	1.46	0.66	0.627	0.166	0.189	Liu et al. (2014)
V410 Aur	0.36636	0.144	SP	1.270	1.37	0.59	0.290	0.154	0.136	Luo et al. (2017)
HN UMa	0.38260	0.145	SP	1.279	1.42	0.61	0.285	0.153	0.132	Oh et al. (2007)
KIC 2159783	0.37388	0.147	T	1.451	1.496	0.694	0.800	0.162	0.095	Senavcı et al. (2016)
TYC 4157-0683-1	0.39607	0.15	T	1.367	1.499	0.667	0.763	0.157	0.115	Acerbi et al. (2014)
V1179 Her	0.38551	0.153	T	1.300			0.450	0.151	0.112	Broens (2021)

observed in clusters with an age spanning 1–6 Gyr and hence it is difficult to reason the possible merger time of AH Cnc in M67 which has an age of ∼4 Gyr (Pols et al. 1998). AH Cnc is an evolved system as it has a low mass ratio $q = 0.161$ and this configuration is plausibly due to the effect of TRO and variable AML. EV Cnc is a member of the cluster (Gao 2018), with a possible semi-detached binary with a mass ratio $q = 0.41$, and is likely to evolve toward a classical Algol system configuration from a contact configuration as the period is found to be increasing. It is clear that EV Cnc and AH Cnc are at different stages of evolution in terms of mass ratio even though they are members of the same cluster.

7. Conclusions

We studied two variables, EV Cnc and AH Cnc, in open cluster M67 using JCBT, TESS and Kepler data. The photometric solutions suggest that EV Cnc is a short period semi-detached binary with a mass ratio $q = 0.41$ and the asymmetry in the light curves can be explained by the presence of hot and cool spots. Based on the $O - C$ studies, we confirm that the orbital period is increasing with a $dp/dt = 2.28 \times 10^{-7}$ days yr^{-1} which is well in agreement with other such similar systems. Photometric solutions of AH Cnc are well in agreement with previous studies, however we did not find any signature of the presence of spots over the stellar surface. Based on the simulations, we estimated the orbital period of the third body to be around $P_3 = 26.82 \pm 2.54$ yr along with an eccentricity $e_3 = 0.67 \pm 0.07$. Future photometric and spectroscopic observations are needed to confirm these results.

Acknowledgments

The authors acknowledge the referee for providing useful comments. Mamatha Rani acknowledges the support from the SRF INSPIRE (IF 170314) fellowship program, Government of India. K.S. and Deblina Lahiri acknowledge financial support from the SERB Core Research Grant project, the Government of India. The authors acknowledge the Director of the Indian Institute of Astrophysics for allocating the time for observations from the JCBT 1.3 m, telescope, Vainu Bappu Observatory. This paper includes data collected with the TESS and Kepler/K2 missions, obtained from the MAST data archive at the Space Telescope Science Institute (STScI). Funding for the TESS mission is provided by the NASA Explorer Program. Funding for the Kepler mission is provided by the NASA Science Mission Directorate. STScI is operated by the Association of Universities for Research in Astronomy, Inc., under NASA contract NAS 5-26555. Gaia data are being processed by the Gaia Data Processing and Analysis Consortium (DPAC). Funding for the DPAC is provided by national institutions, in particular, the institutions participating in the Gaia Multilateral Agreement (MLA). The Gaia mission website is https://www.cosmos.esa.int/gaia. The Gaia archive website is https://archives.esac.esa.int/gaia.

Data Availability

Ground-based observation data are available from the authors and can be provided based on the need and request. TESS and Kepler data are available on the MAST data archive at the Space Telescope Science Institute (STScI).

ORCID iDs

Vijaya, A. https://orcid.org/0000-0003-4852-1756

References

Acerbi, F., Barani, C., & Martignoni, M. 2014, NewA, 31, 1
Alton, K. B. 2018, JAVSO, 46, 3
Binnendijk, L. 1970, VA, 12, 217
Blake, R. M. 2002, PhD Thesis, Canada: York University
Bradstreet, D. H., & Guinan, E. F. 1994, ASPC, 56, 228
Broens, E. 2021, MNRAS, 501, 4935
Chen, X. D., Deng, L. C., de Grijs, R., et al. 2016, AJ, 152, 129
Csizmadia, S., Zhou, A. Y., Konyves, V., Varga, Z., & Sandor, Z. 2002, IBVS, 5230, 1
Csizmadia, S., Klagyivik, P., Borkovits, T., et al. 2006, IBVS, 5736, 1
Christopoulou, et al. 2022, MNRAS, 512, 1244
Cohen, O., Drake, J. J., Kashyap, V. L., & Gombosi, T. I. 2009, APJ, 699, 1501
Csák, B., Kiss, L. L., Vinkó, J., & Alfaro, E. J. 2000, A&A, 356, 603
Darwin, G. H. 1879, Proc. R. Soc. Lond., 29, 168
Deb, S., & Singh, H. P. 2011, MNRAS, 412, 1787
Eggleton, P. P. 2010, NewAR, 54, 45
El-Sadek, M. A., Djurasevic, G., Essam, A., et al. 2019, NewA, 69, 21
Gao, X. 2018, ApJ, 869, 9
Gazeas, K. D., Baran, A., Niarchos, P., et al. 2005, AcA, 55, 123
Gazeas, K. D. 2009, CoAst, 159, 129
Gazeas, K. D., Loukaidou, G. A., Niarchos,, P. G., et al. 2021, MNRAS, 502, 2879
Gezer, I., & Bozkurt, Z. 2016, NewA, 44, 40
Gilliland, R. L. 1991, Astrophysics of the Galaxy, Proceedings of the Conference (New York: Davis Press), 265
Guinan, E. F., & Bradstreet, D. H. 1988, in Formation and Evolution of Low Mass Stars, Proc. NATO Adv. Study Institute 241 (Portugal Dordrecht: NATO Advanced Study Institute), 345
Gürol, B., Bradstreet, D. H., Demircan, Y., & Gürsoytrak, S. H. 2015, New Astronomy, 41, 26
Hajdu, T., Borkovits, T., Forgács-Dajka, E., et al. 2019, MNRAS, 485, 2562
He, J. J., Qian, S. B., Soonthornthum, B., et al. 2019, RAA, 19, 056
Hübscher, J., Paschke, A., & Walter, F. 2005, IBVS, 5657, 1
Hut, P. 1980, A&A, 92, 167
Kim, C. H., Song, M. H., Park, J. H., et al. 2019, JASS, 36, 265
Kılıcoglu, T. 2021, A&A, 655, A91
Kjurkchieva, D. P., Popov, V. A., & Petrov, N. I. 2019, AJ, 158, 186
Kjurkchieva, D., Popov, V., Eneva, Y., & Petrov, N. 2020, BlgAJ, 32, 71
Kouzuma, S. 2018, PASJ, 70, 90
Kouzuma, S. 2019, PASJ, 71, 2
Kovacs, G., Hartman, J. D., & Bakos, G. Á 2019, A&A, 631, A126
Krajci, T. 2005, IBVS, 5592, 1
Li, K., Hu, S., Chen, X., & Guo, D. 2017, PASJ, 69, 79
Li, F.-X., et al. 2023, ApJ, 956, 49
Li, X. Z., Liu, L., & Zhang, X. D. 2020, PASJ, 72, 66
Li, X. Z., & Liu, L. 2021, AJ, 161, 35
Li, K., Xia, Q. Q., Hu, S. M., et al. 2018, PASP, 130, 074201
Liu, L., Chen, W. P., Na, W. W., et al. 2014, NewA, 31, 60
Liu, L., Qian, S., Zhu, L., et al. 2017, NewA, 51, 1
Lucy, L. B. 1967, ZA, 65, 89
Lucy, L. B. 1968, ApJ, 151, 1123
Lucy, L. B. 1976, ApJ, 205, 208
Lucy, L. B., & Wilson, R. E. 1979, ApJ, 231, 502
Luo, X., Wang, K., Zhang, X., et al. 2017, AJ, 154, 99

Maceroni, C., & van't Veer, F. 1996, A&A, 311, 523
Molnar, L. A., Van Noord, D. M., Kinemuchi, K., et al. 2017, ApJ, 840, 1
Nakano, S., Nishiyama, K., Kabashima, F., et al. 2008, IAU Circ., 8972, 1
Oh, K. D., Kim, C. H., Kim, H. I., & Lee, W. B. 2007, in ASP Conf. Ser. Vol. 362, The Seventh Pacific Rim Conference on Stellar Astrophysics, ed. Y. W. Kang et al. (San Francisco: ASP), 82
Ostadnezhad, S., Delband, M., & Hasanzadeh, A. 2014, NewA, 31, 14
Peng, Y.-J., Luo, Z.-Q., Zhang, X.-B., et al. 2016, RAA, 16, 157
Pietrukowicz, P., Soszynski, I., Udalski, A., et al. 2017, AcA, 67, 115
Pols, O. R., Schröder, K.-P., Hurley, J. R., Tout, C. A., & Eggleton, P. P. 1998, MNRAS, 298, 525
Poro, A., Zamanpour, S., Hashemi, M., et al. 2021, NewA, 86, 101571
Pribulla, T., & Rucinski, S. M. 2006, AJ, 131, 2986
Pribulla, T., Rucinski, S., & Matthews, J. M. 2008, MNRAS, 391, 343
Prsa, A., & Zwitter, T. 2005, ApJ, 628, 426
Qian, S. B. 2001, MNRAS, 328, 635
Qian, S. B., Liu, L., Soonthornthum, B., Zhu, L. Y., & He, J. J. 2006, AJ, 131, 3028
Qian, S. B., Liu, L., Soonthornthum, B., Zhu, L.-Y., & He, J.-J. 2007, AJ, 134, 1475
Qian, S. B., Jiang, L.-Q., Fernández Lajús, E., et al. 2015a, ApJL, 798, L42
Qian, S. B., Essam, A., Wang, J.-J., et al. 2015b, AJ, 149, 38
Qian, S. B., He, J.-J., Zhang, J., et al. 2017, RAA, 17, 087
Qian, S. B., Zhang, J., He, J.-J., et al. 2018, ApJS, 235, 5
Qian, S. B., Zhu, L.-Y., Liu, L., et al. 2020, RAA, 20, 10
Raghavan, D., McAlister, H. A., Henry, T. J., et al. 2010, ApJS, 190, 1
Rahunen, T. 1981, A&A, 102, 81
Rappaport, S., Deck, K., Levine, A., et al. 2013, ApJ, 768, 33
Rasio, F. A. 1995, ApJ, 444, L41
Ruciński, S. M. 1969, AcA, 19, 245
Rucinski, S. M., Pribulla, T., & van Kerkwijk, M. H. 2007, AJ, 134, 2353
Samec, R. G., Caton, D. B., & Faulkner, D. R. 2020, JAVSO, 48, 62
Saygan, S. 2016, NewA, 46, 94
Selam, S. O., Esmer, E. M., Senavcı, H. V., et al. 2018, ApSS, 363, 34
Senavcı, H. V., Dogruel, M. B., Nelson, R. H., Yılmaz, M., & Selam, S. O. 2016, PASA, 33, e043
Socia, Q. J., Welsh, W. F., Short, D. R., et al. 2018, ApJ, 864, L32
Sriram, K., Malu, S., Choi, C. S., & Vivekananda Rao, P. 2016, AJ, 151, 69
Sriram, K., Malu, S., Choi, C. S., & Vivekananda Rao, P. 2017, AJ, 153, 231
Sriram, K., Malu, S., Choi, C. S., & Vivekananda Rao, P. 2018, AJ, 155, 172
Sriram, K., & Mamatha Rani, G. 2023, RAA, 23, 115020
Stepien, K. 2006, AcA, 56, 199
Stepien, K., & Gazeas, K. 2012, AcA, 62, 153
Stepien, K., & Kiraga, M. 2015, A&A, 577, A117
Szalai, T., Kiss, L. L., Mészáros, S., Vinkó, J., & Csizmadia, S. 2007, A&A, 465, 943
Tout, C. A., & Hall, D. S. 1991, MNRAS, 253, 9
Tylenda, R., Hajduk, M., Kamiński, T., et al. 2011, A&A, 528, A114
Udalski, A. 2003, AcA, 53, 291
van den Berg, A. P., Jacobs, M. H., & de Jong, B. H. 2002, American Geophysical Union in Fall Meeting (Washington, D. C.: American Geophysical Union)
van Hamme, W. 1993, AJ, 106, 2096
vant Veer, F. 1979, A&A, 80, 287
van't Veer, F., & Maceroni, C. 1989, A&A, 220, 128
Vilhu, O. 1982, A&A, 109, 17
Wang, Z. H., Zhu, L. Y., & Yue, Y. F. 2022, MNRAS, 511, 488
Wadhwa, S. S., De Horta, A. Y., Filipović, M. D., et al. 2021b, MNRAS, 501, 229
Wilson, R. E., & Devinney, E. J. 1971, ApJ, 166, 605
Wilson, R. E. 1979, ApJ, 234, 1054
Wilson, R. E. 1990, ApJ, 356, 613
Xiong, J., et al. 2024, ApJS, 270 (2) 20
Yakut, K., & Ibanoglu, C. 2000, IBVS, 5002, 1,
Yakut, K., Zima, W., Kalomeni, B., et al. 2009, A&A, 503, 165
Yang, Y. G., & Qian, S. B. 2015, AJ, 150, 69
Yang, Y. G., Qian, S. B., Zhang, L. Y., Dai, H. F., & Soonthornthum, B. 2013, AJ, 146, 35
Zhai, D. S., Zhang, X. Y., & Zhang, R. X. 1989, AcASn, 14, 40
Zasche, P., Liakos, A., Niarchos, P., et al. 2009, NewA, 14, 121
Zola, S., et al. 2004, AcA, 54, 299
Zola, S., Gazeas, K., Kreiner, J. M., et al. 2010, MNRAS, 408, 464